

STRUCTURAL CHARACTERIZATION OF A BULK AND NANOSTRUCTURED Al-Fe SYSTEM

KARAKTERIZACIJA STRUKTURE OSNOVE IN NANOSTRUKTURE SISTEMA Al-Fe

Abdelhak Fekrache, Mohamed Yacine Debili, Saliha Lallouche

LM2S, Physics department, Faculty of Science, Badji Mokhtar-Annaba University, 23200 Annaba, Algeria
mydebili@yahoo.fr

Prejem rokopisa – received: 2013-08-06; sprejem za objavo – accepted for publication: 2013-11-12

The main purpose of the present paper is a study of the properties of stable and metastable structures of several binary $Al_{1-x}Fe_x$ alloys ($0 < x < 0.92$) made with high-frequency induction fusion and radiofrequency (13.56 MHz) cathodic sputtering from composite Al-Fe targets, resulting in homogeneous thin films. The study of the lattice parameters and mechanical behaviour was followed by X-ray diffraction and Vickers microhardness measurements of bulk and sputtered Al-Fe thin films. The phenomenon of a significant mechanical strengthening of the aluminium by means of iron is essentially due to a combination of the solid-solution effects and the grain-size refinement. A further decrease in the thin-film grain size can cause a softening of the solid and then the Hall-Petch relation slope turns from positive to negative at a critical size called the strongest size, which is coherent with the thin-film dislocation density.

Keywords: aluminium alloys, sputtering, microhardness, thin films, grain size, Hall-Petch

Glavni namen te predstavitev je študij lastnosti stabilnih in metastabilnih struktur v več binarnih zlitinah $Al_{1-x}Fe_x$ (x -vrednosti so v molskih deležih $0 < x < 0,92$), izdelanih z visokofrekvenčnim zlitvanjem in radiofrekvenčnim (13,56 MHz) katodnim naprševanjem iz kompozitnih tarč Al-Fe, ki omogočajo homogene tanke plasti. Po študiju mrežnih parametrov in mehanskih lastnosti je bila izvršena rentgenska difrakcija in določena mikrotrodota po Vickersu osnove in napršene tanke plasti Al-Fe. Pojav občutnega povečanja mehanske trdnosti aluminija z železom je zaradi kombinacije med vplivi trdne raztopine in zmanjšanja velikosti zrn. Nadaljnje zmanjšanje zrn v tanki plasti lahko povzroči mehčanje in potem se smer razmerja Hall-Petch obrne od pozitivnega k negativnemu pri kritični velikosti, za katero je značilna največja koherenca z gostoto dislokacij v tanki plasti.

Ključne besede: aluminijeve zlitine, naprševanje, mikrotrodota, tanke plasti, velikost zrn, Hall-Petch

1 INTRODUCTION

The characterization of solidification microstructures is essential in many applications. However, the composition complexity of most technical alloys makes such an analysis quite difficult. Microcrystalline and nanocrystalline materials can currently be produced with several methods, like the rapid solidification (RS) or physical vapor deposition (PVD), and the resulting metal has a polycrystalline structure without any preferential crystallographic grain orientation. Aluminium and its alloys with their low densities and easy working have a significant place in the car industry, aeronautics and food conditioning. The on-glass-slides, sputter-deposited, aluminium-based, alloy thin films such as Al-Mg,¹ Al-Ti,^{2,3} Al-Cr⁴ and Al-Fe⁵⁻⁷ exhibit a notable solid solution of aluminium in the films and microhardness values higher than those of the corresponding traditional alloys.

The inverse Hall-Petch effect (IHPE) has been observed for nanocrystalline materials by a large number of researchers.^{8,9} This effect implies that nanocrystalline materials get softer as the grain size is reduced below its critical value. In this paper, we report on a study of the inverse Hall-Petch effect with respect to a practical question as to whether ductility is increased in high-strength metals.

The goal of this paper is to highlight the particular structural behaviours of different Al-Fe alloys prepared by RF magnetron sputtering on glass substrates in terms of structure, lattice parameter, grain size, dislocation density and deviation from the normal Hall-Petch relation.

2 EXPERIMENTAL DETAILS

The eight bulk samples used in the present work, shown in **Table 1**, were quenched from the liquid state after high-frequency induction fusion. Powder aluminium and iron (99.999 %) were used in the proportions defined according to the required compositions. The total mass of the samples to be elaborated was between 8 g and 10 g. A cold compaction of the mixed powder (Al-Fe) was achieved to obtain a dense product (60 %), intended for a high fusion frequency (HF). A sample densified in this way was then placed in a cylindrical alumina crucible (height of 3 cm and diameter of 16 mm), introduced into a quartz tube and placed in the coil prior to the high-frequency fusion. After the primary vacuum, the heating of the sample was carried out in steps, with a ten-minute maintenance stage towards 600 °C until the complete fusion of the alloys at a temperature of about 1140 K, as determined with a pyrometer.

Table 1: Chemical compositions of the bulk and the sputtered Al-Fe alloys (amount fractions, $x/\%$)**Tabela 1:** Kemijska sestava osnove in napršene zlitine Al-Fe (množinski deleži, $x/\%$)

	$x(\text{Fe})/\%$											
Bulk	5.09	10.78	17.16	30	40	60	74	85				
Sputtered	5.6	7.8	18	23	27	29	36	39	47	70	71.9	71.9

Light microscopy (using a Philips microscope) was used for the polished surface observations. The microstructure of the alloys was examined on metallographic microsections. The mechanical polishing technique involved 600–4000 SiC grinding paper. The samples were etched for 15 s with Keller's reagent (5 mL HF + 9 mL HCl + 22 mL HNO₃ + 74 mL H₂O). X-ray diffraction analyses were performed using a Philips X-ray diffractometer working with a copper anticathode ($\lambda = 0.154$ nm) and covering 180° in 2θ . The samples were subjected to heat treatments in primary vacuum media at 500 °C for a period of 1 h.

The twelve targets used in the elaboration of the aluminium-iron thin films were made from a bulk aluminium crown of 70 mm of diameter in which is inserted a bulk copper or iron disc. Using bulk material minimizes the oxygen in the films. This target shape enables the easy control of an additional element composition in the films (**Table 1**).

The films were on 75 mm × 25 mm × 1 mm glass slides that were radiofrequency (13.56 MHz) sputter-deposited under low pressure of 0.7 Pa and a substrate temperature that does not exceed 400 K. The substrate–target distance was 80 mm. The sputtering is carried out with a constant power of 200 W, an auto-polarization voltage of –400 V, that acquired by the plasma is –30 V, a regulation intensity of 0.5 A and a argon flow of 30 cm³/min. After 1 h and 30 min, the deposition velocity is 2.5 $\mu\text{m}/\text{h}$ and films of about 3 μm to 4 μm thickness were obtained.

The chemical analysis of atomic Fe in Al-Fe was made by X-ray dispersion spectroscopy. The microstructure of the films was studied by X-ray diffraction (XRD) using a Philips X-ray diffractometer working with a cobalt $K\alpha$ anticathode ($\lambda = 0.179$ nm) and covering 120° in 2θ , and transmission electronic microscopy (Philips CM12) operating under an accelerating voltage of 120 kV. The Vickers indentation under low load allows us to specify by means of the microhardness the mechanical strengthening of the aluminium by iron addition. The measures were realized by means of a Matsuzawa MTX microdurometre. To reach the intrinsic hardness of the deposit and free itself from the influence of the substrate, the Bückle law¹⁰ must be taken into account. This law imposes a depth of penetration h that does not exceed a tenth of the thickness e of the deposit. So, to have $h < 0.1 e$, it is necessary to respect the condition $D < 0.7 e$, where D is the diagonal of the square impression left by the Vickers indenter (pyramid of angle in the summit equal to 136 °). We chose to work with a normal load of 0.1 N (10 g). In addition, the deposit had to have a

thickness of at least 10 μm so that the previous condition was satisfied.

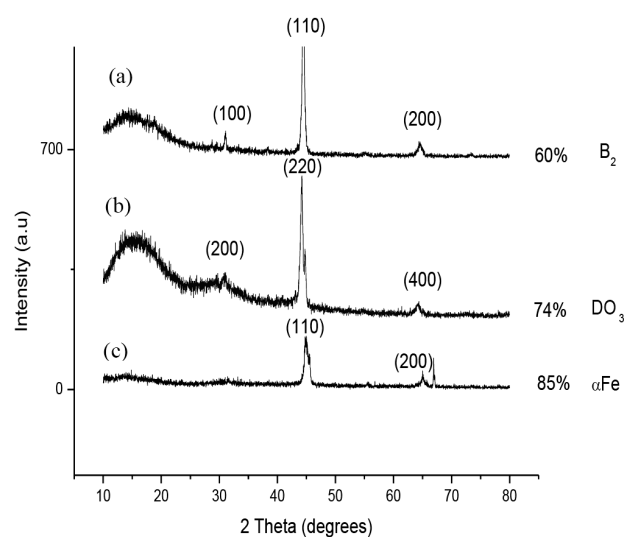
Thin film specimens were sealed in silica ampoules in an argon atmosphere, after a previous evacuation to a pressure of 1.33×10^{-6} mbar, and then heat treated at 500 °C for a period of 1 h.

3 RESULTS AND DISCUSSION

The liquid-quenched Al-60 % Fe alloy is characterized by an ordered B₂ (FeAl) CsCl-type structure, as revealed by the X-ray diffraction pattern (**Figure 1a**), and described in **Table 2**. For 74 % Fe we observe a structural change leading to a DO₃-ordered structure (**Figure 1b**), while when the iron content reaches 85 % and as showed by X-ray diffraction pattern of **Figure 1c**, the structure changes completely, giving rise a disordered α -Fe solid solution (**Figure 2** and **Table 2**).

Table 2: Phase limits in bulk Al-Fe produced by high-frequency induction fusion**Tabela 2:** Fazne meje v osnovi iz Al-Fe, izdelani z visokofrekvenčnim indukcijskim zlitanjem

α -Al Al ₃ Fe	α Al + Al ₃ Fe	α Al + Al ₃ Fe + Al ₆ Fe	α Fe + Al ₂ Fe + Al ₃ Fe ₂	B ₂ + Al ₂ Fe	B ₂	DO ₃	α -Fe
0	20	40	60	60	60	80	100

**Figure 1:** X-ray diffraction patterns of various as-solidified Fe-rich alloys: a) B₂, b) DO₃ and c) α -Fe**Slika 1:** Posnetki rentgenske difrakcije različnih strjenih z Fe bogatih zlitin: a) B₂, b) DO₃, c) α -Fe

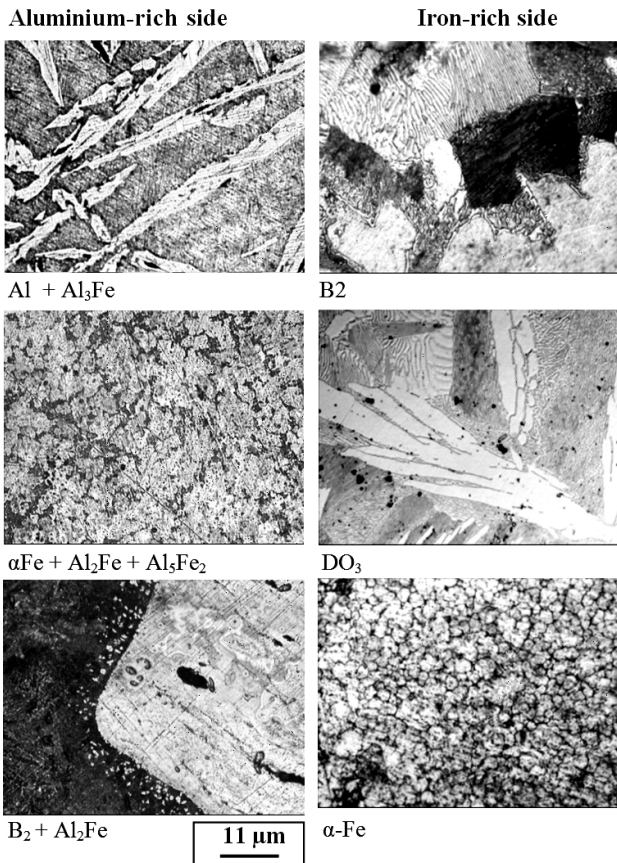


Figure 2: As-quenched microstructures from bulk Al-Fe
Slika 2: Kaljena mikrostruktura osnove iz Al-Fe

For sputtered Al-Fe, the lattice parameter of the α -Al phase decreases from 0.405 nm (pulverized pure aluminium deposit) to 0.403 nm (pulverized deposit containing $x(\text{Fe}) = 5\%$). This decrease in the parameter is not surprising since the radius of the iron atom ($R_{\text{Fe}} = 0.124$ nm) is lower than that of the aluminium atom ($R_{\text{Al}} = 0.143$ nm).

The lattice parameter of the body-centred-cubic phase or the B₂ phase (in the composition field $x(\text{Fe}) = 45\text{--}55\%$) decreases in an appreciably linear way between $x(\text{Fe}) = 38\%$ ($x(\text{Al}) = 62\%$) ($a = 0.295$ nm) and pure iron ($a = 0.287$ nm) while passing the value $a = 0.291$ nm for the pulverized deposit containing $x(\text{Fe}) = 70\%$ ($x(\text{Al}) = 30\%$) (Figure 3). This decrease is again explained by the difference in size between the aluminium and iron atoms.

With the fraction of Al increasing, the bulk Al-Fe lattice parameter increases linearly, which indicates that the Al simply substitutes for Fe on the Fe sublattice. There is a change of slope that occurs at 20% Fe, but when the percentage of Fe is larger than 20%, the lattice parameter decreases, which may indicate that these compositions are in a two-phase field, where the BCC-to-FCC transition may occur between 30% and 40% Fe, see the inset in Figure 3. Similar results were obtained by Pike et al.¹¹ The results clearly indicate that the larger

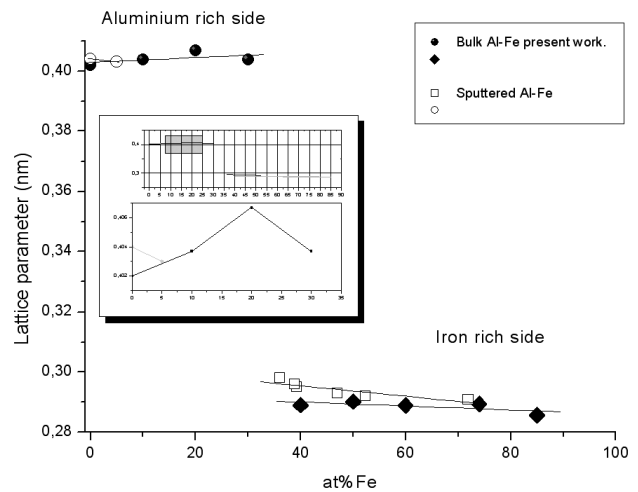


Figure 3: Lattice-parameter variation with iron composition on the aluminium-rich side and iron-rich side. Inset shows a change of the slope for 20% iron.

Slika 3: Spreminjanje mrežnih parametrov s količino železa na z aluminijem bogati strani in z železom bogati strani. Vloženi diagram prikazuje spremembo naklona pri $x(\text{Fe}) = 20\%$

Fe atom preferentially occupies the anti-structure sites on the Al sublattice, and only when these are filled do the Fe atoms begin to occupy the vacancy sublattice.

Between amount fractions 10% and 20% Fe, the bulk alloy microhardness remains almost constant. Beyond 20% Fe it will begin increasing until a maximum at 40% Fe (Figure 4). We observed a Gaussian-shaped curve for the as-solidified alloys. The effect of iron on the mechanical properties of aluminium alloys has been reviewed extensively.^{12,13} The detrimental effect of iron on the ductility is due to two main reasons: 1) the size and number density of iron-containing intermetallics like Al₃Fe and Al₂Fe increases with iron content, and the more intermetallics there are, the lower the ductility; 2) as the iron-level increases, the porosity increases, and this defect also has an impact on the ductility (Table 2).

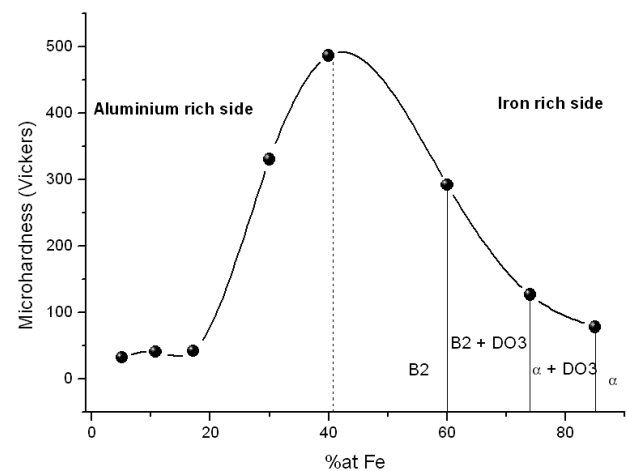


Figure 4: Microhardness evolution with iron content for bulk Al-Fe
Slika 4: Spreminjanje mikrotrdot z vsebnostjo železa v osnovi iz Al-Fe

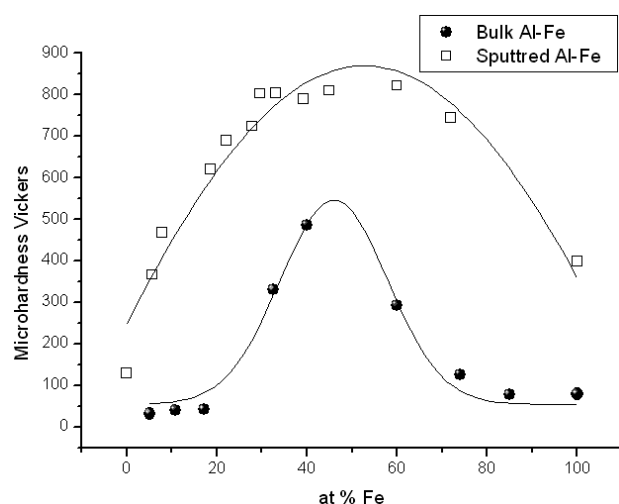


Figure 5: Comparative microhardness variations with iron content for bulk and sputtered Al-Fe

Slika 5: Primerjava spremembe mikrotvrdote z vsebnostjo železa v osnovi in v napršenem Al-Fe

For the Al-Fe deposits the intrinsic microhardness of the thin films increases according to the content of iron from 130 HV (pure aluminium) up to a maximum in the form of plate of 800 HV, located between 45 % and 70 % Fe, and then follows a decrease to reach that of iron towards 400 HV (**Figure 5**).

We have shown in previous work^{6,14} that in aluminium-based thin films the microhardness is always related to the structural and sub-structural features via the influence of the technological physical conditions of vapour condensation and film growth.

3.1 Grain size

Two methods were used for the quantitative approach of the grain size. The first is the application of the Scherer formula.¹⁵ This is based on a measure of the width of the X-ray diffraction field via a measurement of the angular width $\Delta(2\theta)$. The crystallites average dimension being given by $\langle D \rangle = 0.9\lambda/\Delta(2\theta(\cos\theta))$, where λ is the wavelength of the radiation used, θ is the angular position of the diffraction line and $\Delta(2\theta)$ is the width with half intensity expressed in radians. This method assumes the exploitation of diagrams obtained in $\theta/2\theta$ focusing mode with a low divergence of the incident beam. In order to limit the errors, diagrams on aluminium and iron with coarse grains (several micrometres) allowed a free from the instrumental widths of the lines (111) α Al and (110) bcc (body centred cubic) which was used. The results that come from this method provide a good estimate of the grain size when the grain is smaller than 1 μm .

The second method consists of evaluating the grain size starting from images obtained using transmission electron microscopy (**Figure 6**). The evolution of the α -Al grain size in the presence of iron is similar to that already observed in the presence of chromium or

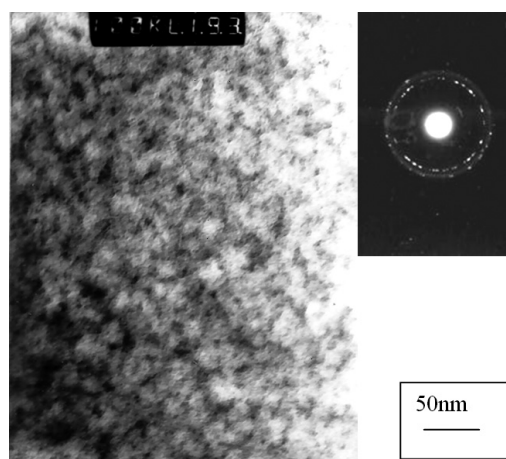


Figure 6: Bright-field transmission electron micrographs and associated selected-area diffraction ring pattern showing a mixture of nanocrystalline and amorphous phases from an Al-7.5 % Fe deposit

Slika 6: Posnetek mikrostrukture s presevnim elektronskim mikroskopom in izbrano področje difrakcije, ki prikazuje mešanico nanokristaliničnih in amorfnih faz v nanosu iz Al-7,5 % Fe

titanium.^{3,4} Whereas the grain of a pulverized pure aluminium deposit has a size of about 1 μm , this falls to approximately 500 nm for $x(\text{Fe}) = 5\%$. Beyond this composition, the microstructure in the two-phase field (α -Al + amorphous) becomes increasingly fine with grains whose dimensions do not exceed 30 nm to 40 nm (**Figure 7**). The refinement of the microstructure, in cathodic sputtering, at the time of the addition of an alloy element in aluminium, is constant, because this element is substituting in the solid solution^{5,14} or inserting in the aluminium.¹⁶

Concerning the body-centred-cubic phase and the ordered B_2 simple cubic phase observed for iron concentrations higher than $x = 38\%$,¹⁷ the grain size varies slightly with iron content in the range of the composition

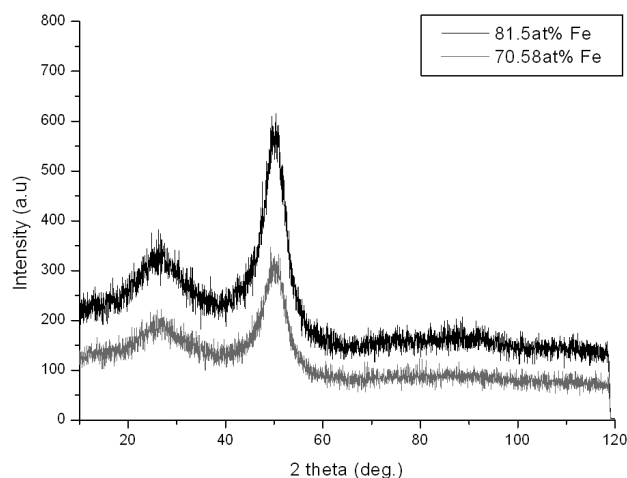


Figure 7: X-ray diffraction pattern of wholly amorphous Al-81.5 % Fe deposit and quasi-amorphous Fe-70.5 % Al deposit

Slika 7: Posnetek rentgenske difrakcije popolnoma amorfnega nanosa Al-81,5 % Fe in kvazi amorfnega nanosa iz Al-70,5 % Fe

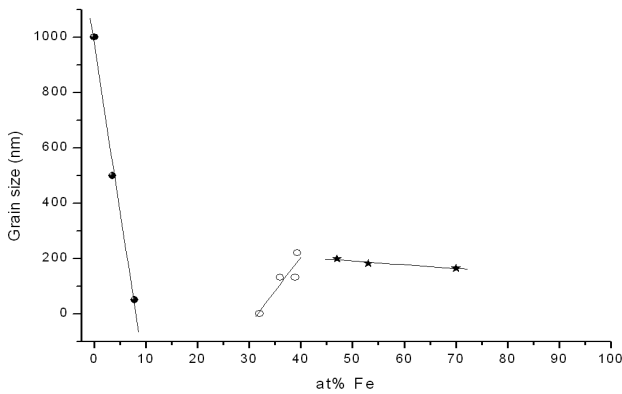
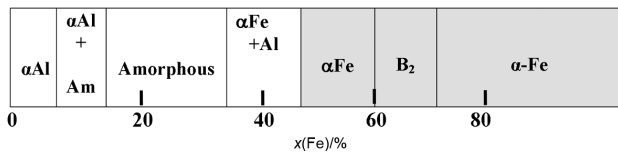


Figure 8: Grain size evolution with iron content
Slika 8: Spreminjanje velikosti zrn od vsebnosti železa

studied (38 % to 72 % Fe) and lies between 200 nm and 250 nm (**Figure 8** and **Table 3**).

Table 3: Phase limit in deposits
Tabela 3: Meje faz v nanosih



For Al-Fe films containing between amount fractions 30 % and 40 % iron we observe an inverse evolution of the Hall-Petch relationship (IHPR) (**Figure 9**).

However, as the crystal is refined from the micrometre regime into the nanometre scale, this mechanism will break down because the grains are unable to support dislocation pile-ups. Typically, this is expected to occur for grain sizes below 10 nm for most metals.¹⁸

There is a growing body of experimental evidence for such unusual deformations in the nanometre regime; however, the underlying atomistic mechanisms for the

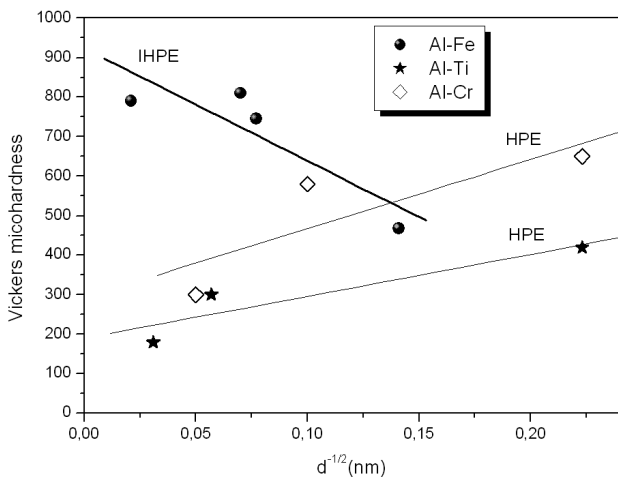


Figure 9: Variation of microhardness with the inverse square root of the grain size

Slika 9: Spreminjanje mikrotvrdote z inverzno vrednostjo kvadratnega korena velikosti zrn

IHPR remain poorly understood. The physical origin of the IHPR transition and the factors dominating the strongest size are a long-standing puzzle.¹⁹

Two main plausible hypotheses have been advanced to explain the deviation from the Hall-Petch relation. First in the HPR regime, crystallographic slips in the grain interiors govern the plastic behaviour of the polycrystallite; while in the IHPR regime, grain boundaries dominate the plastic behaviour. This hypothesis is supported by recent computer simulations of deformation in ultrafine-grained material.²⁰ However, it is not clear from these simulations that grain-boundary sliding could become dominant at grain sizes as large as 20 nm; a recent simulation for Cu suggests a transition at 6–7 nm.⁹ Second, very small grains cannot support distributions of dislocations, so the pile-up and dislocation-density mechanisms for Hall-Petch behaviour cease to apply. Relevant experimental work has recently been published by Misra et al.²¹

3.2 Dislocation density

The finer the grains, the larger the area of the grain boundaries that impedes the dislocation motion. Furthermore, grain-size reduction usually improves toughness as well. The dislocation density for Al-Fe thin films has been determined by using the Williamson and Smallman method.²² Between amount fractions 7.8 % Fe and 36 % Fe, the dislocation density of heat-treated thin films is more sensitive to iron than in the as-deposited specimen (**Figure 10**). This phenomenon may be explained by the relatively small grain size of the as-prepared coatings. From 36 % Fe the dislocation density drops drastically, probably due to the structural change of the coatings from a mixture αAl (fcc) or αFe (bcc) with an amorphous phase to crystalline (bcc) phase. This behaviour is coherent with the inverse Hall-Petch effect (IHPE)

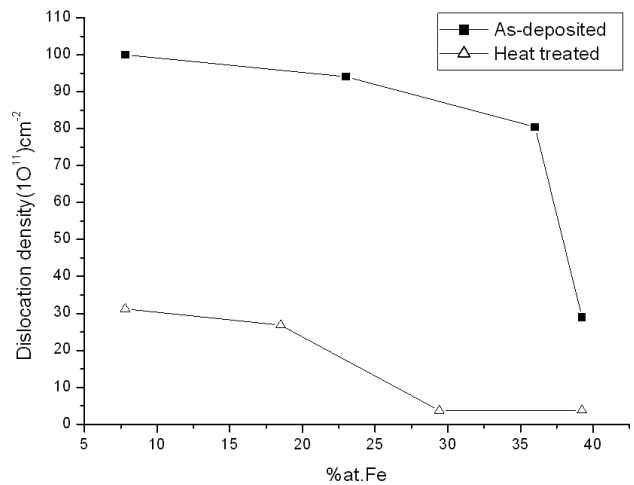


Figure 10: Dislocation density versus iron content for as-deposited and annealed Al-Fe thin films

Slika 10: Gostota dislokacij v odvisnosti od vsebnosti železa za nanesene in žarjene tanke plasti Al-Fe

observed in the same iron concentration range. However, as the crystal is refined from the micrometre scale into the nanometre scale, this mechanism will break down because the grains are unable to support dislocation pile-ups.

The dislocation density after a subsequent heat treatment of the coatings decreases in nearly the same manner as in the as-deposited state until 36 % Fe. Beyond this composition the variation become very slight, because the grain has reached its micrometre size

3.3 Micro deformation

There are several methods (we chose that of Williamson and Hall²³) that can determine the average grain size (D) and the average microstrain rate (ϵ).

For aluminium compositions between amount fractions 30 % and 70 %, the microstrain coming from the tension stress varies smoothly. Beyond 70 % Al the variation become more pronounced, until 90 % Al, and corresponds to the amorphous domain phase. For aluminium compositions higher than 90 %, the microstrain falls again in the domain of α -Al solid solution (**Figure 11**).

A transition of the microstrain from tensile to compressive can be seen after the subsequent heat treatment at 500 °C for a period of 1h, for amorphous films with an aluminium content between mole fractions 68 % and 90 %.

It is well known that the atomic peening of the growing film by energetic particles is currently believed to favor both a dense morphology and grain size refinement. The energetic particles are not only the sputtered metal atoms, but also the high-energy neutral reflected gas atoms.^{24,25} Both the flux and the energy of the high-energy neutral reflected gas atoms are proportional to the $M_t : M_g$ ratio, where M_t is the atomic mass of the target material and M_g is that of the gas. As the transient

metal (TM) is always heavier than Al, increasing the TM insert size on the target is equivalent to increasing the $M_t : M_g$ ratio, and this leads to an enhancement of the in-situ bombardment of the growing film.

4 CONCLUSION

The analysis of the main experimental results issued from the present study leads to an extended solid solution in sputtered films versus liquid quenched alloys and significant mechanical strengthening of the aluminium by means of iron, essentially due to a combination of solid-solution effects and grain-size refinement. The lattice-parameter change of slope that occurs at 20 % Fe in a bulk alloy may indicate that the BCC-to-FCC transition may occur between amount fractions 30 % and 40 % Fe.

The bulk alloy microhardness is related to the detrimental effect of iron on the ductility. The Gaussian increase in the hardness of the alloys as the Fe content increases is explained by the intermetallic Al_3Fe and Al_2Fe phase formation. These phases are found in an eutectic-like structure over a wide composition range, while for Al-Fe deposits, the intrinsic microhardness of the thin films increases in a parabolic way according to the content of iron.

A transition of the microstrain from tensile to compressive can be seen after the heat treatment at 500 °C for a period of 1 h, for amorphous films with aluminium contents between mole fractions 68 % and 90 %.

On an other hand, the dislocation density is observed to exhibit a decreasing trend in both the as-deposited and heat-treated specimens. From 36 % Fe the dislocation density drops sharply, probably due to the structural change of the coatings from a mixture αAl (fcc) or αFe (bcc) with an amorphous phase to a crystalline (bcc) phase. This behaviour is in line with the inverse Hall-Petch effect (IHPE) observed for the same concentration range of iron.

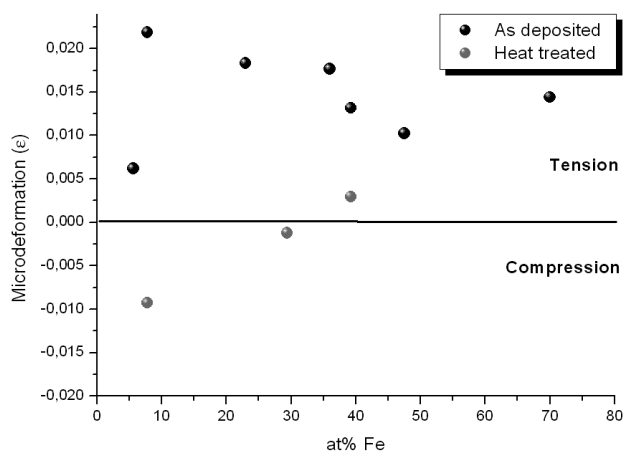


Figure 11: Micro-deformation evolution of as-deposited and heat-treated films with aluminium content

Slika 11: Odvisnost mikrodeformacije nanosenih in toplotno obdelanih plasti od vsebnosti aluminija

5 REFERENCES

- ¹ R. D. Arnell, R. I. Bates, *Vacuum*, 43 (1992), 105
- ² T. Uesugi, Y. Takigawa, K. Higashi, *Mat. Sci. Forum.*, 561–565 (2007), 997
- ³ F. Sanchette, T. H. Loi, A. Billard, C. Frantz, *Surf. Coat. Technol.*, 57 (1993), 179
- ⁴ S. Lallouche, M. Y. Debili, *Proceedings of the 14th European Microscopy Congress*, Aachen, Germany, 2008, 183–184
- ⁵ M. Y. Debili, T. H. Loi, C. Frantz, *Rev. Metall.*, 29 (1998), 1501–1509
- ⁶ M. Y. Debili, *Proc. of the 10th Inter. coll. of french microscopy society*, Grenoble, 2007, 627–641
- ⁷ D. Wu, J. Zhang, J. C. Huang, H. Bei, T. G. Nieh, *Scripta Mater.*, 68 (2013), 118–121
- ⁸ S. Yip, *Nature*, 391 (1998), 532
- ⁹ J. Schiotz, F. D. Di Tolla, K. W. Jacobsen, *Nature*, 391 (1998), 561
- ¹⁰ H. Bückle, *Met. Rev.*, 4 (1959), 49

- ¹¹ L. M. Pike, I. M. Anderson, C. T. Liu, Y. A. Chang, *Acta Mater.*, 50 (2002), 3859
- ¹² L. A. Narayanan, F. H. Samuel, J. E. Gruzaleski, *Metallurgical and Materials Transactions A*, 26 (1995), 2161–2173
- ¹³ L. A. Narayanan, F. H. Samuel, J. E. Gruzaleski, *Metallurgical and Materials Transactions A*, 25 (1994), 1761–1773
- ¹⁴ N. Boukhris, S. Lallouche, M. Y. Debili, M. Draissia, *The European Physical Journal Applied Physics*, 3 (2009), 30501
- ¹⁵ A. Guinier, *Théorie et Technique de la radiocristallographie*, 3rd ed., Dunod, Paris 1964, 461
- ¹⁶ M. Draissia, M. Y. Debili, *CEJP*, 3 (2005), 395–408
- ¹⁷ P. Visuttipitukul, T. Aizawa, H. Kuwahara, *Materials Transactions*, 44 (2003), 2695–2700
- ¹⁸ H. Yoshioka, Q. Yan, K. Asami, K. Hashimoto, *Mat. Sci. Eng.*, 134 (1991), 1054–1057
- ¹⁹ D. Jang, M. J. Atzmon, *Appl. Phys.*, 93 (2003), 9282
- ²⁰ Y. M. Wang, M. W. Chen, F. H. Zhou, E. Ma, *Nature*, 419 (2002), 912
- ²¹ A. Misra, M. Verdier, H. Kung, M. Nastasi, J. D. Embury, J. P. Hirth, *Ultrafine Grained Materials*, R. S. Mishra, et al., eds., TMS, Warrendale, PA (2000), 299
- ²² G. K. Williamson, R. Smallman, *Phil. Mag.*, 1 (1956), 34
- ²³ G. K. Williamson, W. H. Hall, *Acta Metall.*, 1 (1953), 22
- ²⁴ H. Windischmann, *Crit. Rev. Solid State Mater. Sci.*, 17 (1992), 547
- ²⁵ M. Draissia, M. Y. Debili, *Journal of Metastable and Nanocrystalline Materials*, 22 (2004), 121